

Adaptive Interactive Segmentation for Multimodal Medical Imaging via Selection Engine

Zhi Li¹, Kai Zhao², Yaqi Wang^{3*}, Shuai Wang^{1*}

¹Hangzhou Dianzi University, Hangzhou, China

²Department of Neurosurgery, First Medical Center, Chinese PLA General Hospital, Beijing, China

³Communication University of Zhejiang, Hangzhou, China

Abstract—In medical image analysis, achieving fast, efficient, and accurate segmentation is essential for automated diagnosis and treatment. Although recent advancements in deep learning have significantly improved segmentation accuracy, current models often face challenges in adaptability and generalization, particularly when processing multi-modal medical imaging data. These limitations stem from the substantial variations between imaging modalities and the inherent complexity of medical data. To address these challenges, we propose the Strategy-driven Interactive Segmentation Model (SISeg), built on SAM2, which enhances segmentation performance across various medical imaging modalities by integrating a selection engine. To mitigate memory bottlenecks and optimize prompt frame selection during the inference of 2D image sequences, we developed an automated system, the Adaptive Frame Selection Engine (AFSE). This system dynamically selects the optimal prompt frames without requiring extensive prior medical knowledge and enhances the interpretability of the model’s inference process through an interactive feedback mechanism. We conducted extensive experiments on 10 datasets covering 7 representative medical imaging modalities, demonstrating the SISeg model’s robust adaptability and generalization in multi-modal tasks. The project page and code will be available at: <https://github.com/RicoLeehdu/SISeg>.

Index Terms—Multimodal Medical Image Segmentation, Segment Anything, Interactive Segmentation.

I. INTRODUCTION

Medical image segmentation plays a critical role in clinical practice, supporting essential tasks such as diagnosis, treatment planning, and disease monitoring [1]. Accurate segmentation of tissues, organs, and lesions from medical images not only improves diagnostic precision but also enhances treatment planning [2]. However, manual segmentation is a labor-intensive, time-consuming process requiring substantial expertise. In clinical settings, the extensive manual annotation effort renders segmentation inefficient and costly [3]. To overcome these limitations, semi-automatic and fully automatic segmentation methods have emerged, aiming to improve segmentation consistency and efficiency by minimizing manual intervention, thus facilitating the analysis of large-scale medical imaging data [4].

In recent years, deep learning models have propelled interactive segmentation methods to the forefront, particularly in scenarios that require real-time feedback and efficient annotation [4]. By allowing users to provide minimal key

cues, such as bounding boxes around lesions or positive and negative sample points, models can automatically propagate segmentation results without extensive labeling [5], [6], [8]. This is particularly beneficial in medical image segmentation, where real-time interaction can significantly boost clinician productivity, reduce labeling costs, and enhance performance in sequence data processing [9].

While the Segment Anything Model 2 (SAM2) [11] has demonstrated impressive generalization and interactive segmentation capabilities in natural image tasks, it faces significant challenges when applied to medical imaging [27], [28]. Medical images often exhibit complex textures, variable contrasts, and artifacts, making it difficult for a single prompt type to generalize effectively across modalities [9]. Moreover, medical image segmentation frequently involves processing large-scale 2D or 3D sequences [7], where conventional models struggle to balance segmentation accuracy, inference efficiency, and memory consumption [10].

To address these challenges, we propose a strategy-driven intelligent interactive segmentation system (SISeg), designed to adaptively handle multi-modal medical image segmentation. SISeg integrates multiple prompt types and builds upon the Segment Anything Model 2 framework. At the core of SISeg is the Adaptive Frame Selection Engine (AFSE), which dynamically selects the most appropriate prompt frames based on image characteristics, without relying on prior medical knowledge. This engine not only reduces memory consumption but also enhances interpretability in the segmentation process, particularly for sequential data. By incorporating an unsupervised scoring mechanism, SISeg effectively processes diverse modalities such as dermoscopy, endoscopy, and ultrasound, achieving superior segmentation accuracy even in complex scenarios. This work presents three main contributions:

- A novel, flexible multi-prompt segmentation framework (SISeg) that efficiently handles diverse medical imaging modalities without requiring extensive domain-specific knowledge.
- The introduction of the Adaptive Frame Selection Engine (AFSE), which dynamically optimizes prompt frame selection, significantly improving inference efficiency while reducing memory usage.
- Extensive experiments on 10 datasets across 7 distinct medical imaging modalities, validating the superior generalization capability and reduced annotation burden of the SISeg framework.

*Corresponding authors: Yaqi Wang @wangyaqi@cuz.edu.cn and Shuai Wang @shuaiwang.tai@gmail.com.

II. RELATED WORK

A. Segment Anything Model in Medical Imaging

Medical foundation models are large-scale, pre-trained models designed for rapid customization through fine-tuning or in-context learning [10], [12]–[14]. Despite substantial progress, challenges remain in tasks such as image segmentation, largely due to the scarcity of annotated masks [9]. These limitations hinder SAM’s performance, particularly in cross-modal segmentation tasks, where the impact of different prompt types has not been thoroughly investigated [12]. Approaches like MedSAM [9] and Medical SAM Adapter [15] have attempted to enhance cross-modal segmentation by fine-tuning SAM [5] using bounding box prompts on large medical datasets. However, these methods remain constrained by their focus on a limited set of prompt types across modalities. In response to these challenges, we propose a segmentation strategy that integrates multiple prompt types and evaluate its effectiveness across seven representative medical imaging modalities.

B. Medical Image Segmentation

Medical image segmentation is fundamental in modalities such as CT, MRI, and ultrasound [17]–[19]. Models like U-Net [20] and its variants [21]–[23] have demonstrated exceptional performance in this domain. However, most models lack cross-modal robustness, struggle with large-scale datasets, and require extensive manual tuning, failing to optimize prompt selection or interaction efficiency [24], [25]. To address these challenges, we introduce an automated prompt selection framework that intelligently selects prompt frames without relying on domain-specific medical knowledge, significantly reducing memory usage and enhancing inference efficiency, especially for sequence data.

III. METHODOLOGY

A. Strategic Interactive Segmentation System

Preliminaries. As shown in Fig. 1, SAM2 [11] integrates an image encoder, memory encoder, and memory attention mechanism to enhance segmentation by leveraging both current and historical frame information. The image encoder abstracts the input into an embedded representation, while the memory encoder processes representations from previous frames. The memory attention mechanism integrates historical information to refine segmentation of the current frame. This architecture employs a hierarchical visual Transformer as the encoder and a lightweight bidirectional Transformer as the decoder, combining cue and image embeddings.

In this work, we introduce two key modules to optimize the interactive segmentation process: an unsupervised scoring mechanism (Scorer) and a Selector, which aids in selecting representative frames, as shown in Fig. 1.

B. Exploring Robust Prompts

Prompt-based segmentation, particularly with pre-trained models, has become a standard approach for reducing labeling costs in related tasks. SAM2 extends prompt-based

segmentation to video contexts and has demonstrated strong performance in 3D medical imaging, such as CT and MRI, by treating volumetric data as video streams. However, its potential in 2D medical image segmentation remains underexplored.

We found that SAM2 can effectively apply both One-Prompt and Multi-Prompt segmentation across sets of 2D medical images, treating them as video sequences. In this approach, the model requires only a few well-chosen image prompts to achieve segmentation across the entire image set—a task that proves challenging for other methods. Therefore, we investigated the effectiveness of various prompt types across different medical imaging modalities. The specific prompt types and examples are illustrated in Fig. 1.

C. Adaptive Frame Selection Engine

Single-point segmentation [26] allows users to provide a single hint to the model for an unseen example. This approach capitalizes on the model’s generalization ability without requiring retraining or fine-tuning. While this technique is effective for tasks such as optic disc and cup segmentation in fundus images, it may not generalize well across all medical imaging modalities due to the reliance on easily recognizable prior knowledge in some tasks.

Scoring Formula. To address this limitation, we propose an unsupervised scoring mechanism that evaluates the dataset based on image features, aiding in the selection of representative frames for annotation. Let B represent the brightness score, C the contrast score, E the edge density, H the color histogram similarity, and S the shape similarity. These variables are combined to form a composite score F , which is calculated for each image relative to a reference frame in the dataset. The overall composite score is defined as:

$$F = \alpha \cdot B + \beta \cdot C + \gamma \cdot E + \delta \cdot H + \epsilon \cdot S \quad (1)$$

Where:

- α , β , γ , δ , and ϵ are weights assigned to each feature score.
- B (brightness) is computed as the mean brightness of the grayscale image, normalized to the range [0, 1]:

$$B = \frac{\text{mean}(I_{\text{gray}})}{255} \quad (2)$$

- C (contrast) is defined as the standard deviation of the grayscale pixel intensities:

$$C = \frac{\text{std}(I_{\text{gray}})}{255} \quad (3)$$

- E (edge density) represents the proportion of edge pixels, computed using the Canny edge detector:

$$E = \frac{\text{mean}(I_{\text{edges}})}{255} \quad (4)$$

- H (color histogram similarity) measures the correlation between the HSV histograms of the current image and the reference frame:

$$H = \text{corr}(\text{hist}_{\text{HSV}}(I), \text{hist}_{\text{HSV}}(I_{\text{ref}})) \quad (5)$$

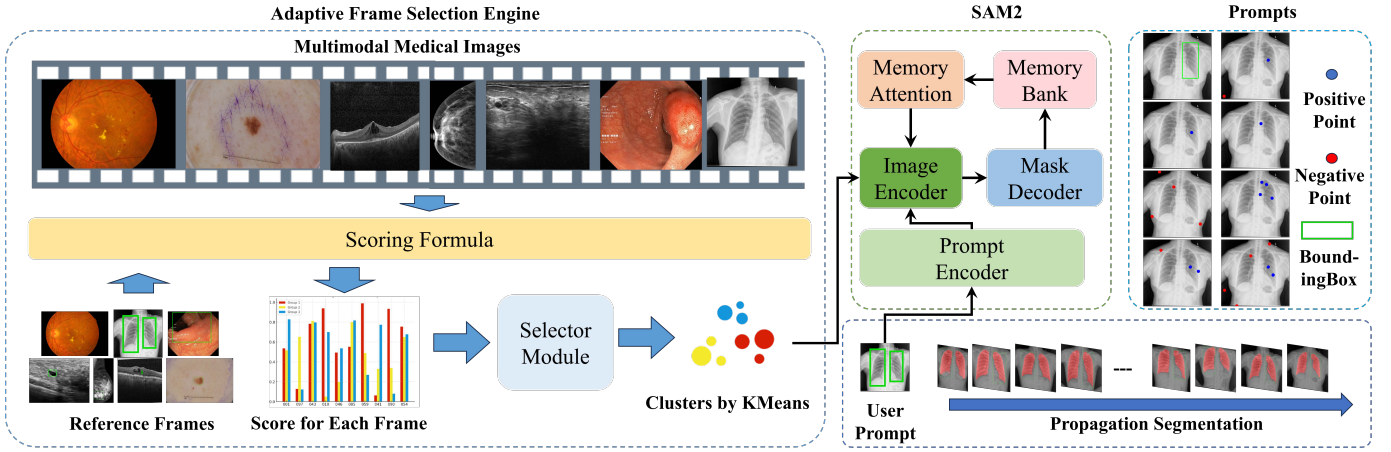


Fig. 1. The model structure of SISeg. The figure illustrates the SAM2 architecture, which includes the image encoder, prompt encoder, memory attention mechanism, streaming memory bank, and mask decoder. AFSE leverages reference frames provided by clinicians to enable fully automated feedback and segmentation propagation. The top-right section highlights an example with chest X-rays, demonstrating the application of various prompt types, such as true negative point prompts and bounding box prompts, for model-based segmentation.

- S (shape similarity) is derived from the Hu moments of the grayscale image and the reference frame, defined as:

$$S = -\log \left(\sum_{i=1}^7 |M_{\text{Hu}}(I_{\text{ref}})_i - M_{\text{Hu}}(I)_i| + \epsilon \right) \quad (6)$$

where M_{Hu} represents the Hu moments, and ϵ is a small constant to prevent division by zero.

The composite score F is calculated for each image, and K-means clustering is applied to group frames into clusters based on their similarity to the reference frame.

Selector Module. The interaction engine incorporates a selector module to enable efficient dataset navigation. The Selector initially identifies a reference frame I_{ref} , chosen by the clinician for its clinical relevance. Each frame in the dataset is then assigned a composite score F , computed based on its similarity to the reference frame. This composite score integrates various features, such as brightness, contrast, edge density, color histogram similarity, and shape similarity, as defined in Equation (1). The process is illustrated in Fig. 1.

To group similar frames, we apply the KMeans clustering algorithm. Given a set of N frames, let $\mathbf{X} = \{F_1, F_2, \dots, F_N\}$ represent the composite scores of these frames. The KMeans algorithm minimizes the following objective function:

$$\min_{C_1, C_2, \dots, C_k} \sum_{i=1}^k \sum_{x \in C_i} \|x - \mu_i\|^2 \quad (7)$$

where C_i is the i -th cluster, and μ_i is the centroid of C_i . The algorithm iteratively minimizes the sum of squared distances between each frame's composite score and its cluster centroid. After clustering, frames closest to the centroids are selected as representative frames for segmentation. The Scorer module then ranks the remaining frames by their proximity to these centroids, providing feedback to the user on the most relevant frames for further annotation.

Subsequently, SISeg automatically propagates segmentation based on the prompts associated with the selected key frames. Figure 1 demonstrates an example of lung segmentation in X-ray mode. This process reduces manual intervention and enhances segmentation efficiency by partitioning long sequence datasets into clusters based on scoring, thereby lowering inference costs.

IV. EXPERIMENTS

A. Experimental Setup

Dataset. In our experiments, we utilized seven distinct medical imaging modalities: Dermoscopy (Der), Endoscopy (Endo), Fundus, Optical Coherence Tomography (OCT), Ultrasound (US), X-ray (XRay), and Mammography (MG). Ten publicly available datasets were employed, including: PAPILA [29], Breast Ultrasound [30], Kvasir-SEG [31], IDRiD [32], ISIC 2018 [33], Intraretinal Cystoid Fluid [34], CDD-CESM [35], m2caiSeg [38], Chest X-ray Masks and Labels [36], and hc18 [37]. Due to inference cost constraints, the datasets were split into training and validation sets using a 7:3 ratio with scikit-learn [39], applying a fixed seed of 2024 to ensure consistency. The validation set comprises 30% of the original data.

Implementation Details. The experiments were conducted on a single RTX 3090 GPU. We employed four pre-trained SAM2 model variants: sam2 hiera tiny, sam2 hiera small, sam2 hiera base plus, and sam2 hiera large, to effectively adapt the model to the medical imaging datasets. The evaluation metrics used for performance assessment were Dice coefficient and Intersection over Union (IoU).

B. Results and Analysis

SAM2 Zero-Shot Performance. Table I presents the segmentation performance of various SAM2 Hierarchical models, evaluated using the Bounding Box prompt across different medical

TABLE I
COMPARISON OF DICE AND IOU SCORES ACROSS DIFFERENT SAM2 HIERA MODEL TYPES FOR VARIOUS MEDICAL IMAGING MODALITIES.

Model Type	Metric	Der	Endo	Fundus	OCT	US	XRy	MG
SAM2 Hiera Tiny	Dice	94.79	85.27	99.92	90.31	94.44	96.55	81.56
	IoU	90.98	77.64	99.88	83.96	90.19	94.01	75.18
SAM2 Hiera Small	Dice	91.84	85.48	99.96	90.25	93.73	96.47	81.26
	IoU	87.39	78.03	99.94	83.93	89.59	93.93	74.63
SAM2 Hiera Base Plus	Dice	94.11	86.24	99.98	90.39	94.51	95.51	80.72
	IoU	90.04	78.59	99.96	84.13	90.36	92.99	73.86
SAM2 Hiera Large	Dice	93.57	93.61	99.98	90.22	94.71	96.48	82.65
	IoU	89.31	90.39	99.96	83.89	90.68	93.98	75.93

TABLE II
COMPARISON OF DICE SCORES ACROSS VARIOUS MODALITIES FOR DIFFERENT SELECTION STRATEGIES. R REPRESENTS THE NUMBER OF REFERENCE FRAMES.

Modality	R	Der	Endo	Fundus	OCT	US	XRy	MG
Random	1	59.84	59.77	99.95	31.99	99.69	42.88	46.34
Uniform	5	50.52	52.41	99.97	30.65	99.83	37.01	43.24
AFSE (wo scorer)	5	62.54	50.83	99.67	23.24	99.76	55.79	39.85
AFSE	5	62.55	60.22	99.75	33.90	99.98	60.07	50.82

imaging modalities. The SAM2 variants exhibited strong zero-shot segmentation performance, with each variant performing optimally in specific modalities, as illustrated in Fig. 2.

Effects of AFSE. The Adaptive Frame Selection Engine (AFSE) consistently outperformed both random and uniform strategies across multiple modalities, as shown in Table II. AFSE’s scoring mechanism ensures that the selected frames are more representative and clinically relevant, leading to improved segmentation accuracy and reduced annotation effort.

Notably, AFSE surpasses the second-best method, AFSE (without scorer), by 9.39% in X-ray and 10.97% in Mammography, underscoring the significance of the scoring mechanism. Additionally, AFSE demonstrates a 6.33% improvement in Endoscopy and a 10.66% improvement in OCT.

C. Ablation Studies

Robust Prompts for SAM2 Propagation Segmentation.

In Table III, we compare the performance of various combinations of positive and negative point prompts with bounding box prompts across different medical imaging modalities. The results show that bounding box prompts, which enclose the target organ or lesion, consistently deliver the best segmentation performance by effectively leveraging SAM2’s propagation mechanism. In contrast, the performance of point-based prompts is highly dependent on the correct combination of positive and negative points.

Scoring Formula. As demonstrated in Table IV, AFSE effectively selects relevant frames for segmentation, significantly improving both efficiency and accuracy. By employing an unsupervised scoring mechanism that evaluates image features such as brightness, contrast, edge density, color histogram similarity, and shape similarity, AFSE automatically selects and ranks frames. This automated approach reduces the need for manual intervention, streamlining the segmentation process, while also maintaining robust generalization across diverse imaging modalities.

TABLE III
COMPARISON OF DICE SCORES ACROSS DIFFERENT PROMPT STRATEGIES AND MEDICAL IMAGING MODALITIES.

Modality	Der	Endo	Fundus	OCT	US	XRy	MG
Standard Pos	82.71	77.25	99.88	63.06	84.56	58.78	58.36
Random Pos	74.36	81.37	99.82	57.48	79.62	52.21	53.11
Single Neg	55.42	45.85	99.62	31.37	54.55	37.33	49.64
Single Pos Neg	82.41	50.94	99.78	61.86	83.29	63.48	58.49
Four Pos	76.07	81.69	99.76	59.14	82.21	51.78	56.19
Four Neg	54.43	00.78	99.61	34.75	50.11	37.54	44.86
Single Pos Two Neg	80.88	88.54	99.87	56.25	83.75	69.21	59.79
Two Pos Four Neg	80.24	54.13	99.87	51.73	82.56	67.41	60.31
BBox	94.79	85.27	99.92	90.31	94.44	96.55	81.56

TABLE IV
COMPARISON OF DICE SCORES FOR DIFFERENT EVALUATION STRATEGIES ACROSS MEDICAL IMAGING MODALITIES. AFSE REPRESENTS A COMPREHENSIVE EVALUATION MECHANISM THAT INTELLIGENTLY COMBINES THESE METRICS.

Modality	Der	Endo	Fundus	OCT	US	XRy	MG
Brightness	62.31	50.41	99.67	22.71	99.78	55.79	39.38
Color Histogram	62.71	51.67	99.67	23.24	99.76	55.79	39.85
Contrast	62.08	51.13	99.67	23.24	99.78	55.79	39.38
Edge Density	63.39	53.71	99.67	22.11	99.75	55.47	39.49
Shape Similarity	62.09	52.89	99.69	24.99	99.77	43.21	41.97
AFSE	62.55	60.22	99.75	33.91	99.83	60.07	50.82

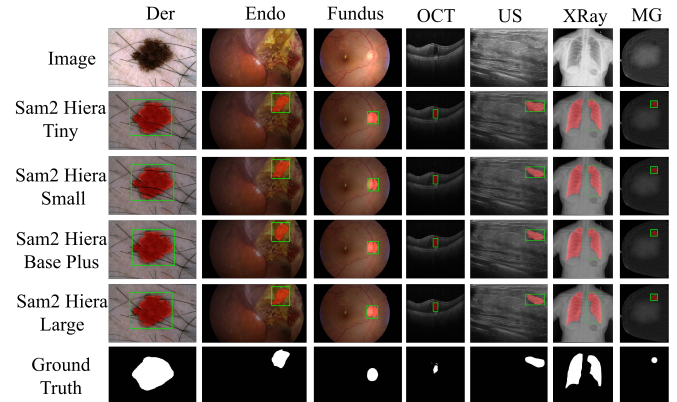


Fig. 2. Visualization of zero-shot segmentation results produced by different SAM2 Hiera models across various medical imaging modalities.

V. CONCLUSION

In this work, we introduce the Strategy-driven Interactive Segmentation Model (SISeg), which enhances medical image segmentation across multiple modalities by integrating diverse prompt types. Using the Adaptive Frame Selection Engine (AFSE), SISeg dynamically selects optimal prompts without requiring prior medical knowledge, reducing memory usage and improving interpretability. Experiments on 10 datasets across 7 modalities show SISeg’s ability to boost segmentation efficiency and lower annotation costs.

VI. ACKNOWLEDGMENTS

This research is supported by the National Natural Science Foundation of China (No. 62201323, No. 62206242), and the Natural Science Foundation of Jiangsu Province (No. BK20220266).

REFERENCES

- [1] F. Isensee, P. F. Jaeger, S. A. A. Kohl, J. Petersen, and K. H. Maier-Hein, "nnU-Net: a self-configuring method for deep learning-based biomedical image segmentation," *Nature Methods*, vol. 18, no. 2, pp. 203–211, 2021.
- [2] J. De Fauw, J. R. Ledsam, B. Romera-Paredes, S. Nikolov, N. Tomasev, S. Blackwell, H. Askham, X. Glorot, B. O'Donoghue, D. Visentin, et al., "Clinically applicable deep learning for diagnosis and referral in retinal disease," *Nature Medicine*, vol. 24, no. 9, pp. 1342–1350, 2018.
- [3] D. Ouyang, B. He, A. Ghorbani, N. Yuan, J. Ebinger, C. P. Langlotz, P. A. Heidenreich, R. A. Harrington, D. H. Liang, E. A. Ashley, et al., "Video-based AI for beat-to-beat assessment of cardiac function," *Nature*, vol. 580, no. 7802, pp. 252–256, 2020.
- [4] G. Wang, M. A. Zuluaga, W. Li, R. Pratt, P. A. Patel, M. Aertsen, T. Doel, A. L. David, J. Deprest, S. Ourselin, et al., "DeepGeoS: a deep interactive geodesic framework for medical image segmentation," *IEEE Transactions on Pattern Analysis and Machine Intelligence*, vol. 41, no. 7, pp. 1559–1572, 2018.
- [5] A. Kirillov, E. Mintun, N. Ravi, H. Mao, C. Rolland, L. Gustafson, T. Xiao, S. Whitehead, A. C. Berg, W. Lo, et al., "Segment anything," in *Proceedings of the IEEE/CVF International Conference on Computer Vision*, pp. 4015–4026, 2023.
- [6] G. Wang, W. Li, M. A. Zuluaga, R. Pratt, P. A. Patel, M. Aertsen, T. Doel, A. L. David, J. Deprest, S. Ourselin, et al., "Interactive medical image segmentation using deep learning with image-specific fine tuning," *IEEE Transactions on Medical Imaging*, vol. 37, no. 7, pp. 1562–1573, 2018.
- [7] T. Zhou, L. Li, G. Bredell, J. Li, J. Unkelbach, and E. Konukoglu, "Volumetric memory network for interactive medical image segmentation," *Medical Image Analysis*, vol. 83, pp. 102599, 2023.
- [8] X. Luo, G. Wang, T. Song, J. Zhang, M. Aertsen, J. Deprest, S. Ourselin, T. Vercauteren, and S. Zhang, "MIDeepSeg: Minimally interactive segmentation of unseen objects from medical images using deep learning," *Medical Image Analysis*, vol. 72, pp. 102102, 2021.
- [9] J. Ma, Y. He, F. Li, L. Han, C. You, and B. Wang, "Segment anything in medical images," *Nature Communications*, vol. 15, no. 1, pp. 654, 2024.
- [10] C. Hu, T. Xia, S. Ju, and X. Li, "When sam meets medical images: An investigation of segment anything model (sam) on multi-phase liver tumor segmentation," *arXiv preprint arXiv:2304.08506*, 2023.
- [11] N. Ravi, V. Gabeur, Y.-T. Hu, R. Hu, C. Ryali, T. Ma, H. Khedr, R. Rädle, C. Rolland, and L. Gustafson, et al., "Sam 2: Segment anything in images and videos," *arXiv preprint arXiv:2408.00714*, 2024.
- [12] D. Cheng, Z. Qin, Z. Jiang, S. Zhang, Q. Lao, and K. Li, "Sam on medical images: A comprehensive study on three prompt modes," *arXiv preprint arXiv:2305.00035*, 2023.
- [13] R. Deng, C. Cui, Q. Liu, T. Yao, L. W. Remedios, S. W. Bao, B. A. Landman, L. E. Wheless, L. A. Coburn, K. T. Wilson, et al., "Segment anything model (sam) for digital pathology: Assess zero-shot segmentation on whole slide imaging," *arXiv preprint arXiv:2304.04155*, 2023.
- [14] S. Roy, T. Wald, G. Koehler, M. R. Rokuss, N. Disch, J. Holzschuh, D. Zimmerer, and K. H. Maier-Hein, "Sam. md: Zero-shot medical image segmentation capabilities of the segment anything model," *arXiv preprint arXiv:2304.05396*, 2023.
- [15] S. Chai, R. K. Jain, S. Teng, J. Liu, Y. Li, T. Tateyama, and Y. Chen, "Ladder fine-tuning approach for sam integrating complementary network," *arXiv preprint arXiv:2306.12737*, 2023.
- [16] J. Wu, W. Ji, Y. Liu, H. Fu, M. Xu, Y. Xu, and Y. Jin, "Medical sam adapter: Adapting segment anything model for medical image segmentation," *arXiv preprint arXiv:2304.12620*, 2023.
- [17] Y. Fu, Y. Lei, T. Wang, W. J. Curran, T. Liu, and X. Yang, "A review of deep learning based methods for medical image multi-organ segmentation," *Physica Medica*, vol. 85, pp. 107–122, 2021.
- [18] Y. Wang, Y. Zhou, W. Shen, S. Park, E. K. Fishman, and A. L. Yuille, "Abdominal multi-organ segmentation with organ-attention networks and statistical fusion," *Medical Image Analysis*, vol. 55, pp. 88–102, 2019.
- [19] Y. Ji, H. Bai, C. Ge, J. Yang, Y. Zhu, R. Zhang, Z. Li, L. Zhanng, W. Ma, X. Wan, et al., "Amos: A large-scale abdominal multi-organ benchmark for versatile medical image segmentation," *Advances in Neural Information Processing Systems*, vol. 35, pp. 36722–36732, 2022.
- [20] O. Ronneberger, P. Fischer, and T. Brox, "U-net: Convolutional networks for biomedical image segmentation," in *Medical Image Computing and Computer-Assisted Intervention—MICCAI 2015: 18th International Conference, Munich, Germany, October 5-9, 2015, Proceedings, Part III*, pp. 234–241, Springer, 2015.
- [21] F. I. Diakogiannis, F. Waldner, P. Caccetta, and C. Wu, "ResUNet-a: A deep learning framework for semantic segmentation of remotely sensed data," *ISPRS Journal of Photogrammetry and Remote Sensing*, vol. 162, pp. 94–114, 2020.
- [22] F. Isensee, J. Petersen, A. Klein, D. Zimmerer, P. F. Jaeger, S. Kohl, J. Wasserthal, G. Koehler, T. Norajitra, S. Wirkert, et al., "nnu-net: Self-adapting framework for u-net-based medical image segmentation," *arXiv preprint arXiv:1809.10486*, 2018.
- [23] Z. Zhou, M. M. R. Siddiquee, N. Tajbakhsh, and J. Liang, "Unet++: A nested u-net architecture for medical image segmentation," in *Deep Learning in Medical Image Analysis and Multimodal Learning for Clinical Decision Support: 4th International Workshop, DLMIA 2018, and 8th International Workshop, ML-CDS 2018, Granada, Spain, September 20, 2018, Proceedings 4*, pp. 3–11, Springer, 2018.
- [24] J. Duan, J. Xiong, Y. Li, and W. Ding, "Deep learning based multimodal biomedical data fusion: An overview and comparative review," *Information Fusion*, vol. 102536, 2024.
- [25] Y. Liu, K. Zhang, Y. Li, Z. Yan, C. Gao, R. Chen, Z. Yuan, Y. Huang, H. Sun, J. Gao, et al., "Sora: A review on background, technology, limitations, and opportunities of large vision models," *arXiv preprint arXiv:2402.17177*, 2024.
- [26] J. Wu and M. Xu, "One-prompt to segment all medical images," in *Proceedings of the IEEE/CVF Conference on Computer Vision and Pattern Recognition*, pp. 11302–11312, 2024.
- [27] J. Zhu, Y. Qi, and J. Wu, "Medical sam 2: Segment medical images as video via segment anything model 2," *arXiv preprint arXiv:2408.00874*, 2024.
- [28] J. Ma, S. Kim, F. Li, M. Baharoon, R. Asakereh, H. Lyu, and B. Wang, "Segment anything in medical images and videos: Benchmark and deployment," *arXiv preprint arXiv:2408.03322*, 2024.
- [29] J. Sánchez Ramos, M. Ortega, M. G. Penedo, and N. Barreira, "PAPILA: Dataset with fundus images and clinical data of both eyes of the same patient for glaucoma assessment," *NCBI*, 2022.
- [30] M. C. Medeiros, M. Z. do Nascimento, and G. Carneiro, "BUS-BRA: A breast ultrasound dataset for assessing computer-aided diagnosis systems," *PubMed*, 2023.
- [31] D. Jha, P. H. Smedsrud, M. A. Riegler, P. Halvorsen, T. de Lange, D. Johansen, and H. D. Johansen, "Kvasir-SEG: A Segmented Polyp Dataset," *arXiv*, 2019.
- [32] R. Rani and S. K. Sahoo, "Deep Learning Framework Design for Diabetic Retinopathy Abnormalities Classification," *Semantic Scholar*, 2024.
- [33] A. G. C. Pacheco, R. A. Krohling, A. L. D. Rossi, L. S. Oliveira, G. D. C. Cavalcanti, J. P. M. Ferreira, F. M. M. Pereira, R. Marques, S. Avila, and E. Valle, "Deep-Learning Ensembles for Skin-Lesion Segmentation, Analysis, Classification: RECOD Titans at ISIC Challenge 2018," *arXiv*, 2018.
- [34] M. K. Garvin, M. D. Abramoff, R. Kardon, S. R. Russell, X. Wu, and M. Sonka, "Multivendor Spectral-Domain Optical Coherence Tomography Dataset, Observer Annotation Performance Evaluation, and Standardized Evaluation Framework for Intraretinal Cystoid Fluid Segmentation," *NCBI*, 2016.
- [35] J. Maia, I. C. Moreira, I. Ramos, M. J. Cardoso, and J. S. Cardoso, "Categorized contrast enhanced mammography dataset for diagnostic and artificial intelligence research," *NCBI*, 2022.
- [36] Z. Jiang, Y. Shen, Y. Jiang, Y. Ding, and Y. Ding, "CheXmask: a large-scale dataset of anatomical segmentation masks for multi-center chest x-ray images," *arXiv*, 2023.
- [37] T. L. A. van den Heuvel, D. de Bruijn, C. L. de Korte, and B. van Ginneken, "Automated measurement of fetal head circumference using 2D ultrasound images," *PloS one*, vol. 13, no. 8, pp. e0200412, 2018.
- [38] S. Maqbool, A. Riaz, H. Sajid, and O. Hasan, "m2caiSeg: Semantic Segmentation of Laparoscopic Images using Convolutional Neural Networks," *arXiv preprint arXiv:2008.10134*, 2020.
- [39] F. Pedregosa, G. Varoquaux, A. Gramfort, V. Michel, B. Thirion, O. Grisel, M. Blondel, P. Prettenhofer, R. Weiss, V. Dubourg, J. Vanderplas, A. Passos, D. Cournapeau, M. Brucher, M. Perrot, and E. Duchesnay, "Scikit-learn: Machine Learning in Python," *Journal of Machine Learning Research*, vol. 12, pp. 2825–2830, 2011.